Appl Biochem Biotechnol (2009) 156:489–505
DOI 10.1007/s12010-008-8486-7

Periodic Fermentor Yield and Enhanced Product Enrichment from Autonomous Oscillations

Chris C. Stowers · J. Brian Robertson · Hyunju Ban · Robert D. Tanner · Erik M. Boczko

Received: 8 May 2008 / Accepted: 10 December 2008 /
Published online: 30 January 2009

Abstract Four decades of work have clearly established the existence of autonomous oscillations in budding yeast culture across a range of operational parameters and in a few strains. Autonomous oscillations impact substrate conversion to biomass and products. Relatively little work has been done to quantify yield in this case. We have analyzed the yield of autonomously oscillating systems, grown under different conditions, and demonstrate that it too oscillates. Using experimental data and mathematical models of yeast growth and division, we demonstrate strategies to increase the efficient recovery of products. The analysis makes advantage of the population structure and synchrony of the system and our ability to target production within the cell cycle. While oscillatory phenomena in culture have generally been regarded with trepidation in the engineering art of bioprocess control, our results provide further evidence that autonomously oscillating systems can be a powerful tool, rather than an obstruction.

Keywords Ambient biocomplexity · Protein purification · Enrichment ratio · Mitotic cell cycle

Introduction

Because yeast and other fungi are genetically tractable, double rapidly, and have the ability to post-translationally modify proteins as required for their efficacy as human drugs, they have become an increasingly attractive platform for bioprocessing. Yeast are currently being used to manufacture insulin and hydrocortisone as pharmaceuticals [1–4] and to

C. C. Stowers · R. D. Tanner
Department of Chemical Engineering, Vanderbilt University, Nashville, TN 37235, USA

J. B. Robertson
Department of Biological Sciences, Vanderbilt University, Nashville, TN 37232, USA

H. Ban · E. M. Boczko (✉)
Department of Biomedical Informatics, Vanderbilt University, Nashville, TN 37235, USA
e-mail: erik.boczko@vanderbilt.edu

produce invertase and amylase for the biofuels industry [5, 6]. Despite the evolved efficiency and robustness of cellular processes, most of the biotechnological processes that utilize living cells operate at modest efficiencies [7, 8]. In fact, single steps of the bioproduction process have been shown to be less than 50% efficient [2], whereas the highly developed commodity chemical industry routinely operates at efficiencies greater than 90%.

Inefficiencies arise in protein purification and isolation [9]. For example, products of interest may be produced but not secreted from the cell. Harvesting cellular proteins is challenging. While the cell cycle itself is relatively well understood in yeast, only a limited understanding of its quantitative impact on bioprocess-related parameters exists. For instance, yeast cell disruption has only recently been shown to have strong cell cycle dependence [10]. During and following cell disruption, protein products may be degraded due to the liberation of normally sequestered proteases. Protease knockout strains have been extensively utilized for this reason [11]. Moreover, many proteins share primary through quaternary structural similarities that can confer upon them similar physical–chemical properties that confound their separation and efficient isolation. Most proteins perform their biological functions in complexes and, accordingly, have adapted surface interaction domains. These adaptive features work against efficient isolation.

For the purposes of this paper, we designate the protein background that a protein product of interest is expressed among its *ambient biocomplexity*. The larger and more diverse this background, the higher is its ambient biocomplexity. The confounding effects of proteins that are physically and chemically similar to the desired target product motivate this definition. The more proteins in an admixture that are physically and chemically similar to the desired target product, the more steps will be required to isolate the product away from its mimics or contaminating biomolecules. It stands as self-evident that increased ambient biocomplexity can only reduce bioprocess efficiency. Ambient biocomplexity depends on the target protein and on the method of separation. The ambient biocomplexity of a target T, given separation method M, is a set of molecules, ${}_{M}A^{T}$, that has the following transitive property: if a protein Z is in the set ${}_{M}A^{T}$, then T must be in the set ${}_{M}A^{Z}$. This is because the same physical method is assumed to link the proteins through the behavior dictated by their common properties. This paper is concerned with exploring optimal strategies to reduce a desired products' ambient biocomplexity and consequently increasing its efficient harvest by maximizing its enrichment ratio relative to impurities.

Many proteins can be and are produced in a cell-cycle-dependent manner. The cyclin genes that regulate cell cycle progression are an example. Currently, a detailed proteomic catalog of the type and magnitude of expressed yeast proteins as a function of the cell cycle is not available. It has been shown that total protein production increases throughout the cell cycle [12, 13]. As a consequence, the lowest biocomplexity might occur near the beginning of the G_1 phase of the cell cycle. Such data suggest that biocomplexity might fluctuate as a function of the cell cycle or could be manipulated to do so.

In an asynchronously doubling culture, cell-cycle-dependent products are produced asynchronously, although continuously. It has been observed that periodically harvesting a periodic product can improve yield relative to continuously harvesting from an asynchronous culture [14]. Conventional methods to produce cell cycle synchrony include metabolic blocks involving starvation, mating pheromones such as alpha factor, chemical treatment such as nocodozole, and the preparation of homogeneous initial populations by physical means such as elutriation [15]. Typically, only three to four decaying cycles of synchrony can be achieved with these methods. We have developed continuous filtration methods that guarantee the maintenance of synchrony over 30 consecutive cell cycles, but

these are not yet generally implemented [16]. None of these methods are cost-effective, however, and likely the reason why synchronous yeast cultures are rarely used in industry. However, there is another option.

A few strains of yeast exhibit sustained oscillations under a limited variety of conditions [17]. Autonomously oscillating systems are attractive for at least three reasons. First, the oscillations reflect a form of cell cycle synchrony whose population structure we believe we understand. This level of understanding allows for the opportunity to interleave expression out of phase with ambient biocomplexity. The population synchrony induced via autonomous oscillations ensures that the synchronous fabrication of products occurs with no additional cost. The value of synchronous production of products has been demonstrated with *Bacillus subtilis* [18]. Finally, since autonomous oscillations are stable, often for months, costs associated with quality controlling lots can be reduced, as well as costs associated with production interruptions and restarts incurred during batch processing.

Microbial oscillations have generally been regarded with trepidation due to their perceived instability [19]. Forty years of data and experience show that in fact, autonomous oscillations are highly controllable [20–28]. In fact, we show that they can be used to great advantage. We show that regardless of a product's ambient biocomplexity, there exists an expression profile that produces an accumulation of the product that dramatically improves product yield and its enrichment ratio. Moreover, we show how to utilize parallel, phased periodic sampling to create continuous enrichment in a scheme we have dubbed "CLOCKS". We believe that this point of view is novel. These development are important since downstream processing costs account for over 75% of cost of manufacturing a drug that in turn translates into 1,525% of the retail cost of a bioproduct [29]. Non-growth-associated products, such as the production of alpha amylase from *Bacillus licheniformis* [30], are not subject to the analysis that we present. Non-growth-associated products are produced during the stationary phase of the growth curve during which cells become arrested in the cell cycle and are therefore no longer subject to cell-cycle-dependent production of bioproducts.

Materials and Methods

Autonomous Oscillations

The haploid (mat a) strain CEN.PK 113-7D of *Saccharomyces cerevisiae* was cultivated in a 3L New Brunswick Scientific Bioflow 110 reactor equipped with two Rushton type impellers operated at 550 rpm. Air was sparged in at a rate of 900 mL/min. Temperature was maintained at 30 °C and pH was automatically controlled with 2 N sodium hydroxide.

Overnight cultures were grown in YPD media with shaking. Twenty milliliters was inoculated into a reactor containing 850 mL of synthetic media with the following composition: 10 g/L anhydrous glucose (Sigma no. G71528), 5 g/L ammonium sulfate (Sigma no. A2939), 0.5 g/L magnesium sulfate heptahydrate (Sigma no. M2773), 1 g/L of yeast extract (Becton, Dickinson and Company Cat no. 288620), 2 g/L potassium phosphate (Sigma no. P5379), 0.5 mL L^{-1} of 70% (*v*/*v*) sulfuric acid, 0.5 mL of antifoam A (Sigma no. 10794), 0.5 mL of 250 mM calcium chloride, and 0.5 mL L^{-1} of mineral solution A (see Table 1).

The culture was grown in batch for 12–16 h to a cell density of approximately 5×10^9 cells/mL. Continuous culture ensued with a dilution rate of 0.095 h^{-1} to promote autonomous oscillation [22]. Samples were taken from the reactor and flash-frozen using dry ice.

Table 1 A list of components and their respective concentration within the mineral solution used to prepare culture media for CEN.PK 113-7D.

Mineral solution A	
$FeSO_4 \cdot 7H_2O$	40 g/L
$ZnSO_4 \cdot 7H_2O$	20 g/L
$CuSO_4 \cdot 5H_2O$	10 g/L
$MnCl_2 \cdot 4H_2O$	2 g/L
75% H_2SO_4	20 mL/L

Measurement of Cell Density

Cell samples were thawed in a chilled (4 °C) sonicating water bath for 5 min and vortexed briefly. A 1-μL sample was resuspended in 10 mL of Isoton diluent (Sigma no., Beckman Coulter no. 8546719) and vortexed. The cell density of three independent half milliliter samples was measured using a Beckman Multisizer Coulter counter. The sizing threshold was 2–8 μm.

Measurement of Bud Index

Samples were collected at 15-min intervals and immediately frozen in an ethanol–dry ice bath. Buds were counted with a 100× objective on a conventional Nikon TE-2000 microscope. A minimum of 300 cells were scored at each time point. Cells without buds were considered to be within the G_1 phase of the cell cycle.

Calculation of Yield

Yield was computed by solving the mass balance for substrate.

$$Y(X,S) = \frac{\mu X}{D[S_F - S] - \frac{dS}{dt}} \tag{1}$$

where Y represents the yield of cells per unit of substrate, μ is the population growth rate, X is the cell density, S is the substrate concentration, S_F is the concentration of the substrate in the feed, and D is the dilution rate. A similar equation can be derived to represent the yield of cells in terms of the dissolved oxygen content:

$$Y(X,O_2) = \frac{\mu X}{D[O_{2F} - O_2] - \frac{dO_2}{dt}}. \tag{2}$$

The population growth rate, μ, was determined from cell biomass and cell number data assuming the model (Table 2):

$$\mu = \frac{1}{X}\frac{dX}{dt} + D. \tag{3}$$

The data of Heinzle et al. [25] were linearly interpolated to account for differences in sampling times and frequency. All numerical manipulations were carried out using Mathematica version 5.2 from WolframResearch. The dissolved oxygen trace was recorded every 12 s. The dissolved oxygen measurements displayed both high-frequency

Table 2 Parameter values used to evaluate Eqs. 1, 2, and 3.

Parameter values		
Parameter	Value	Units
$S_{F,Glucose}$ [35]	20	g/L
$S_{F,Glucose}$ (current exp.)	10	g/L
$S_{F,Oxygen}$	7.6	mg/L

measurement noise and rapid oscillation. Five measurements per minute were averaged to produce a data set of 391 measurements covering one cell cycle. These data points were fit with a cubic spline using the interpolation function. The analytical derivative of the interpolation was contaminated with high-frequency noise. Two options were considered: Further smooth the raw oxygen data or smooth the derivative. Since the derivative correctly captured the global features of the oxygen oscillations and further smoothing of the raw data could lead to small temporal shifts of relevant features, we present the latter solution. Comparison of the methods showed no qualitative difference. The dissolved oxygen derivative data were smoothed using a Gaussian kernel in ListConvolve, with a standard deviation corresponding to a 2.5-min time window and no overhangs.

The cell density is a slowly varying function of the cell cycle. The density data were collected every 15 min and were not contaminated with high-frequency noise. The data were interpolated with a cubic spline. The growth rate was calculated according to Eq. 3 using the analytical derivative of the interpolating function. A dilution rate of 0.095 h^{-1} and an oxygen feed of 100% were assumed using the yield formula presented in Eq. 2.

Results

Analysis of Fermenter Yield

Yield describes the gain in a product per unit input. Yield coefficients have been an important benchmark of fermenter efficiency for over 30 years [23]. The yield of cell mass in terms of glucose substrate, $Y_{X/S}$, and dissolved oxygen $Y_{X/O2}$, were computed from the data of Heinzle et al. [25] (see Fig. 1) for the yeast strain LBGH-1022 (see Fig. 2). The yield, $Y_{X/O2}$, was calculated independently for the strain Cen.PK from data collected in our laboratory (see Fig. 3). The combined results indicate that the yield oscillates with a period equal to that of the dissolved oxygen. We are unaware of any published results of this nature. Since substrate concentration is linked to growth rate, large substrate oscillations are likely to entrain cell cycle synchrony [14] and oscillating yield. The magnitude of the yield is influenced by the phase of the substrate oscillation relative to that of product/biomass, with the largest amplitude occurring when the signals are perfectly out of phase. In the case of the Heinzle et al. data [25], the glucose profile is nearly in phase with the biomass, whereas the oxygen profile is far out of phase, as shown in Fig. 1. As a result, $Y_{X/O2}$ is larger in amplitude than $Y_{X/S}$. Many compounds, such as ethanol, glycogen, NADPH, and acetaldehyde, have been shown to oscillate during long period aerobic oscillations in several strains [25, 28]. Therefore, it is expected that the yield with respect to these compounds oscillates periodically as well.

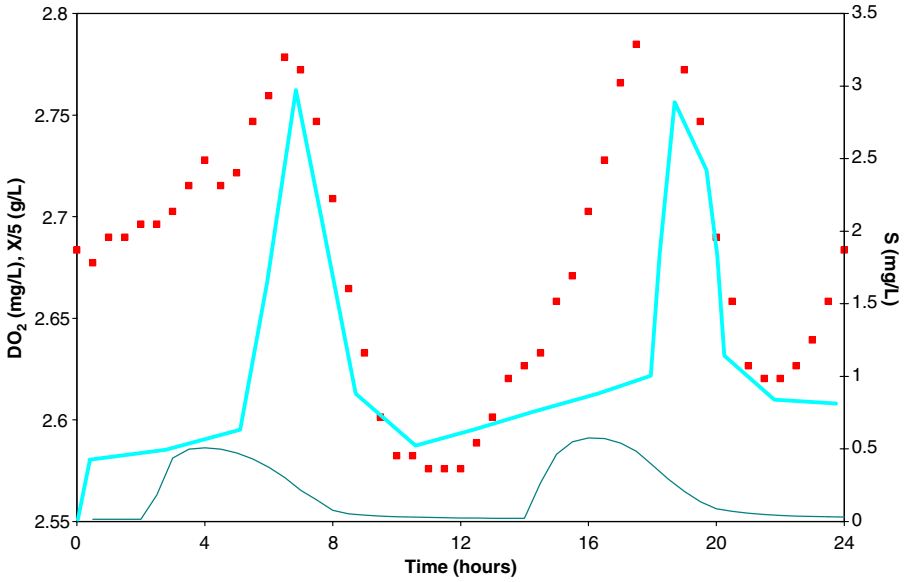

Fig. 1 Bioprocess data from Heinzel et al. [25]. The dissolved oxygen concentration (*thin line*) peaks before the glucose concentration (*solid blue*). The biomass (*red squares*) peaks roughly in phase with the substrate glucose. The biomass data are scaled to accommodate the data within the same figure

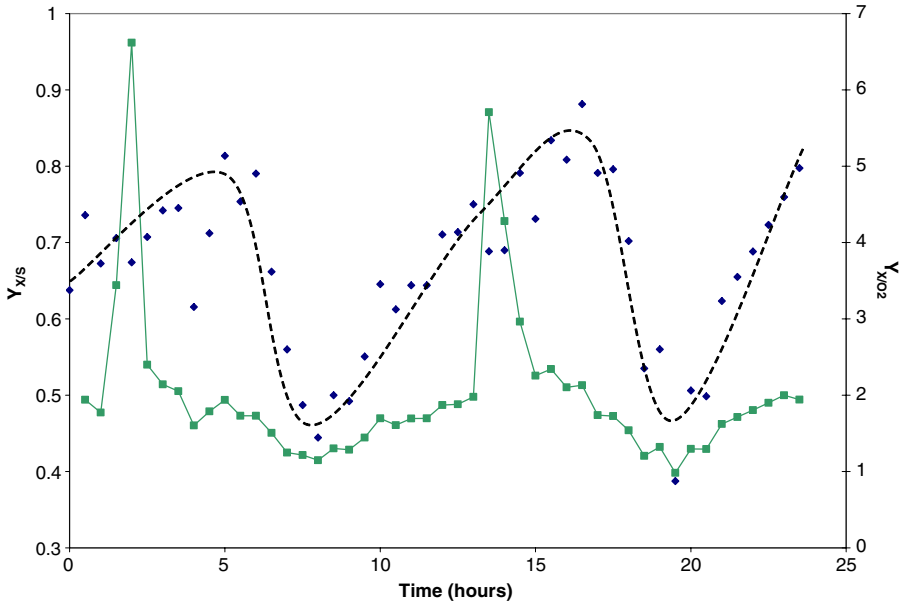

Fig. 2 The time-dependent biomass yield relative to glucose consumption computed from the data of Heinzle et al. [25], shown in Fig. 1, using Eqs. 1 and 3. The *blue data points* and *dashed black line* represent the yield of biomass (grams of biomass per gram of glucose) relative to the glucose concentration. The *green data points* and *trace* represent the biomass yield with respect to oxygen concentration (grams of biomass per milligram of oxygen). These data imply product yield oscillation

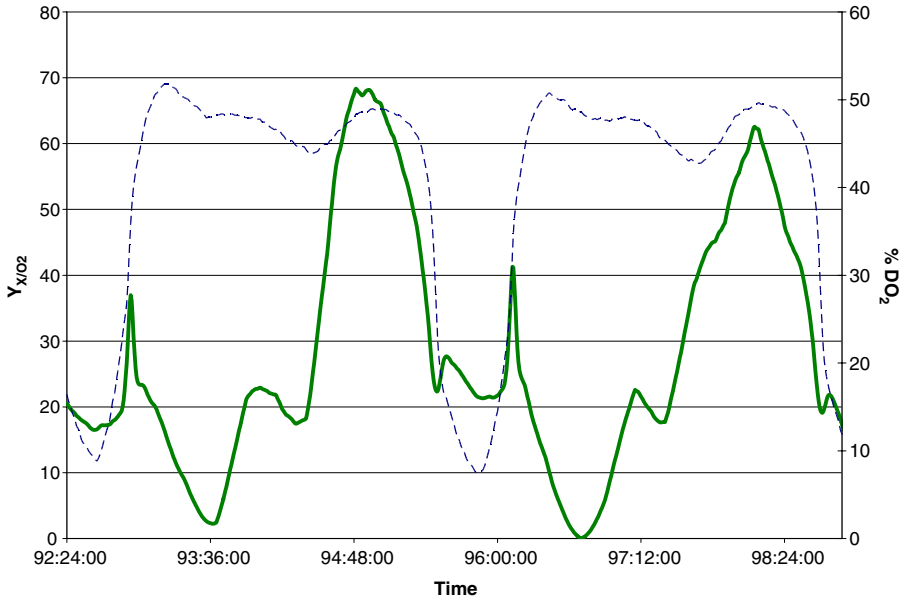

Fig. 3 Complex, periodic biomass yield oscillation as a function of dissolved oxygen consumption. $Y_{X/O2}$ (*green*) computed using data shown in Fig. 5 and Eq. 3 as described in the text. In this case, $Y_{X/O2}$ is not dimensionless and has the units of cells per % DO_2. Dissolved oxygen is shown in *dashed blue*. Time is shown as hours:minutes:seconds elapsed since culture inception. The figure spans a total of 390 min

Population Structure, Biocomplexity, and the Product Enrichment Ratio

An analysis of the bud index and cell number time series demonstrate that autonomous oscillations in strain Cen.PK 113-7D are integrally linked to the cell cycle (see Figs. 4 and 5). The link being that the cell population is divided into temporally coherent clusters of cells that travel around the cell cycle almost exactly out of phase with regard to bud emergence and division (see Fig. 6). Figure 4 demonstrates that during the low portion of a dissolved oxygen oscillation, nearly all of the cells exist within the G_1 portion of the cell cycle. This follows a maximum in the cell density, indicating that a wave of cell division has just ended (see Fig. 5). With no new increase in cell number, the percentage of cells in G_1 subsequently falls to 50%, indicating that one of the two clusters has passed into the S-phase of the cell cycle. The steepness of the transition indicates the temporal cohesion of the cell population that comprises half the total number of cells. Since each culture doubling time is marked by exactly two oscillations in the bud index and the cell density, it is concluded that the population structure under autonomous oscillations is as depicted in Fig. 6.

Figure 7 depicts a phase portrait of biomass versus glucose (substrate) concentration. The oscillatory nature of the system produces a counterclockwise orbit in the phase plane space that we have annotated with respect to suspected total biocomplexity. The annotation is based on the observation that biomass increases exponentially around the cell cycle. The G_1 portion of the cell cycle may be a time of low biocomplexity.

The term ambient biocomplexity of a product is meant to highlight the problem that product separation costs dominate bioproduction. In any scheme to isolate a product from an admixture, each successive step is designed to enrich the product relative to background.

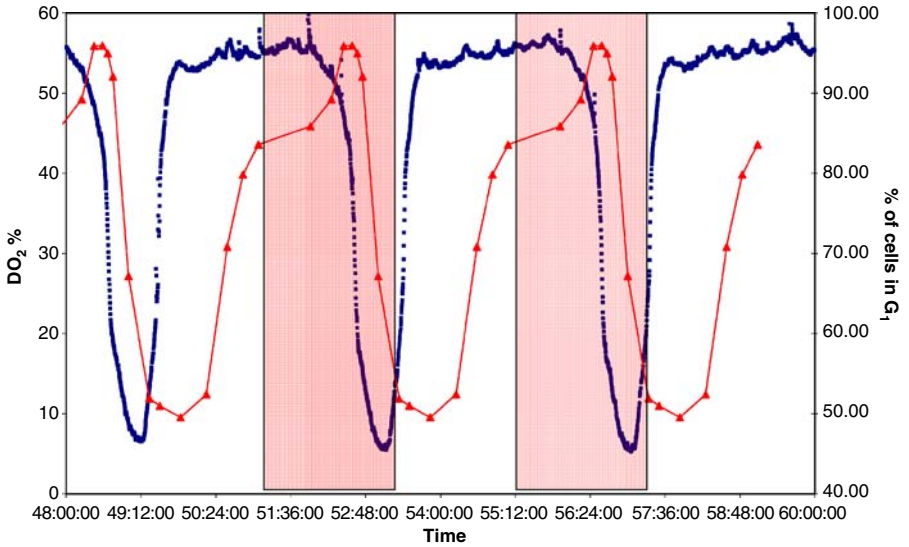

Fig. 4 Autonomous oscillations of Cen.PK 113 in a 3-L bioreactor operated at D=0.088 h^{-1}. Dissolved oxygen, as the percentage of saturation, is shown in *blue*. The fraction of cells in the G_1 phase of the cell cycle are plotted as *red triangles*. The *red shaded regions* represents a maximal G_1 harvesting window within the oscillation. As described in the text, this harvesting window may represent a minimum in total biocomplexity. The complement of the bud index data represents the percentage of cells in G_1 [34, 35]. The bud index data were recorded over the central dissolved oxygen oscillation and its periodic extension is shown

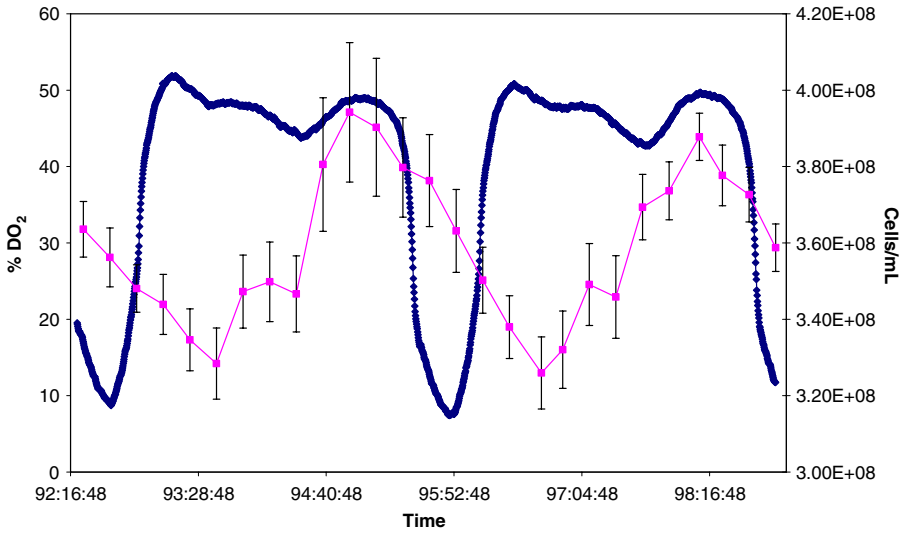

Fig. 5 Cell density time series. Cell density (*squares*) was measured at regular 15-min intervals across two 3.5-h dissolved oxygen oscillations that together constitute a doubling time under an imposed dilution rate of D=0.095 h^{-1}. Cell density as measured with a Coulter counter changes as a function of division and dilution. The data indicate a concerted division event precedes each wave of respiration. *Error bars* represent the standard deviation of the measurement. Time is shown as hours:minutes:seconds elapsed since culture inception. The figure spans a total of 390 min

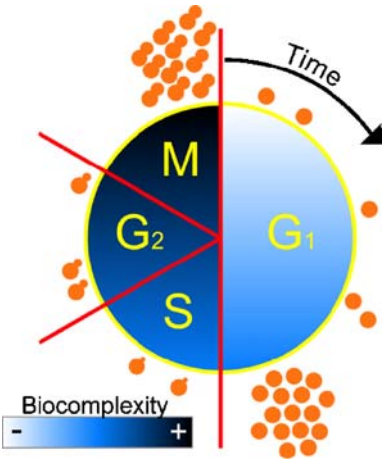

Fig. 6 Population structure and biocomplexity of autonomous oscillations. Two clustered cell populations are arranged around a schematic of the budding yeast cell cycle in accordance with the data from Figs. 4 and 5. Cell cycle progression is clockwise, with cell division punctuating the M to G_1 transition. A model of biocomplexity is indicated through shading according to the data of [12, 13]

In the case of a protein product, it is reasonable to equate the ambient biocomplexity with the total protein content of the cell. Some work indicates that the internal protein complexity of a cell increases with cell cycle position [12, 13]. Isolation of a protein product from a cell sample at a time of its lowest biocomplexity is by definition guaranteed to maximize its enrichment ratio and minimize costs. We present a theoretical analysis that illustrates that periodic systems can be gamed to produce a product of interest out of phase with its biocomplexity. This analysis is based on our experimental understanding of the population structure that becomes entrained during autonomous oscillations.

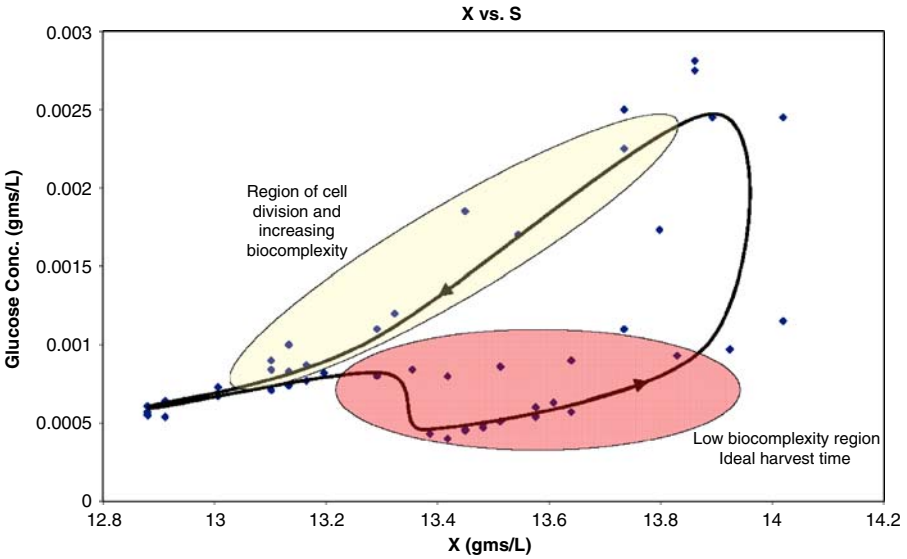

Fig. 7 Phase portrait of a periodic orbit. Biomass (*X*) versus glucose concentration (*S*) corresponding to the Heinzle et al. data of Fig. 4. The *red lower shaded region* encompasses the G_1 period that is characterized by increasing but low total biocomplexity (see also Fig. 6). The *yellow upper shaded region* encompasses the highest biocomplexity. The *arrows* indicate increasing time

Accumulation of Biocomplexity

Let $p(t,s)$ represent a population density stratified according to time t, and cell cycle position, s. Suppose that the cells of the population are producing a protein or an admixture of proteins in a cell-cycle-dependent manner. Let the function $f(s)$ specify a single cell production profile that depends only on the cell cycle position, s. See for instance the sketch in the top panel of Fig. 8. It is well known, and has been repeatedly shown, that the vast majority of transcripts are cell-cycle-dependent [27]. Given the single cell production $f(s)$, and the population density, $p(t,s)$, the instantaneous production is given by their inner product:

$$I(t) = \int p(t,s),f(s)\mathrm{d}s. \tag{4}$$

Furthermore, the products, F, will accumulate within a reactor with dilution rate D, according to a mass balance equation

$$\frac{\mathrm{d}F}{\mathrm{d}t} = I(t) - DF(t). \tag{5}$$

Given the assumption that the population density is a periodic function of time (see Figs. 4, 5, and 6), we show that the function F is asymptotically periodic (see Appendix 1). Furthermore, we demonstrate that regardless of the phase profile of the accumulation function F, we can design a product expression function, $g(s)$, to create a product, G, that is maximally out of phase with the complexity produced by f. The conclusion is twofold. First ambient biocomplexity F will oscillate; and second, that regardless of the ambient biocomplexity, we can design a production scheme that is maximally out of phase with it. This implies that we can maximally enhance the enrichment ratio of G relative to F.

It has been suggested in the literature that the total protein complexity of the cell increases exponentially with the cell cycle [12, 13]. Therefore, as a demonstration of enrichment ratio enhancement, we consider the case where ambient biocomplexity is represented as an increasing exponential function over the cell cycle (see Fig. 8). We compute the evolution of a population of yeast cells with a Leslie type model that is the discrete analog of the popular population balance equations. The Leslie model is extremely flexible in that it allows us to represent a finite but arbitrary number of age classes, is easily parameterized with experimental data of yeast growth relevant parameters, and is computationally tractable. A description of the model is given in Appendix 2. We have previously shown that the Leslie models that we have employed reproduce the dynamics observed in experimental time series [16].

Fig. 8 Maximization of the enrichment ratio. The *upper panel* shows single cell expression rates as a function of their cell cycle. The *lower figure* shows the resulting normalized population expression from a population of cells undergoing autonomous oscillation and expressing individually according to the *upper panel*. The *red curve* represents an arbitrary choice to model a hypothetical ambient biocomplexity that increases exponentially along the cell cycle. The *green* and *blue* punctate expression patterns represent different choices for product expression rates. We call these promoter models. The *arrow above the promoter models* in the *upper panel* highlights the fact that we are examining a sliding window to find an optimal one. The *bottom panel* shows the normalized output in terms of concentration for these expression rates in a population. The population dynamics have been simulated by the Leslie model described in Appendix 2. The *bottom panel* shows that as the punctate windows of the promoter models are shifted, they tile the possible phases of the oscillation (see *arrows* in the *top* and *bottom panels*). Of the promoter models, there exists one that is maximally out of phase with the biocomplexity, highlighted by the *dashed vertical black line*. The *bold blue intervals* along the abscissa correspond to a choice of harvesting windows induced by imposing a complexity threshold indicated by the *dashed horizontal line*

Simulations generated from the Leslie model are shown in the bottom panel of Fig. 8, corresponding to the single cell expression profiles shown in the upper panel. The ambient biocomplexity is depicted in the upper panel of Fig. 8 by the red cell cycle expression profile and in the bottom panel by the red accumulation signal. All of the cells in the population are assumed to be expressing the single cell expression profiles in a cell-cycle-dependent manner as outlined by the equations above and in the appendices to produce the corresponding accumulation profiles. The green and blue single cell expression profiles in

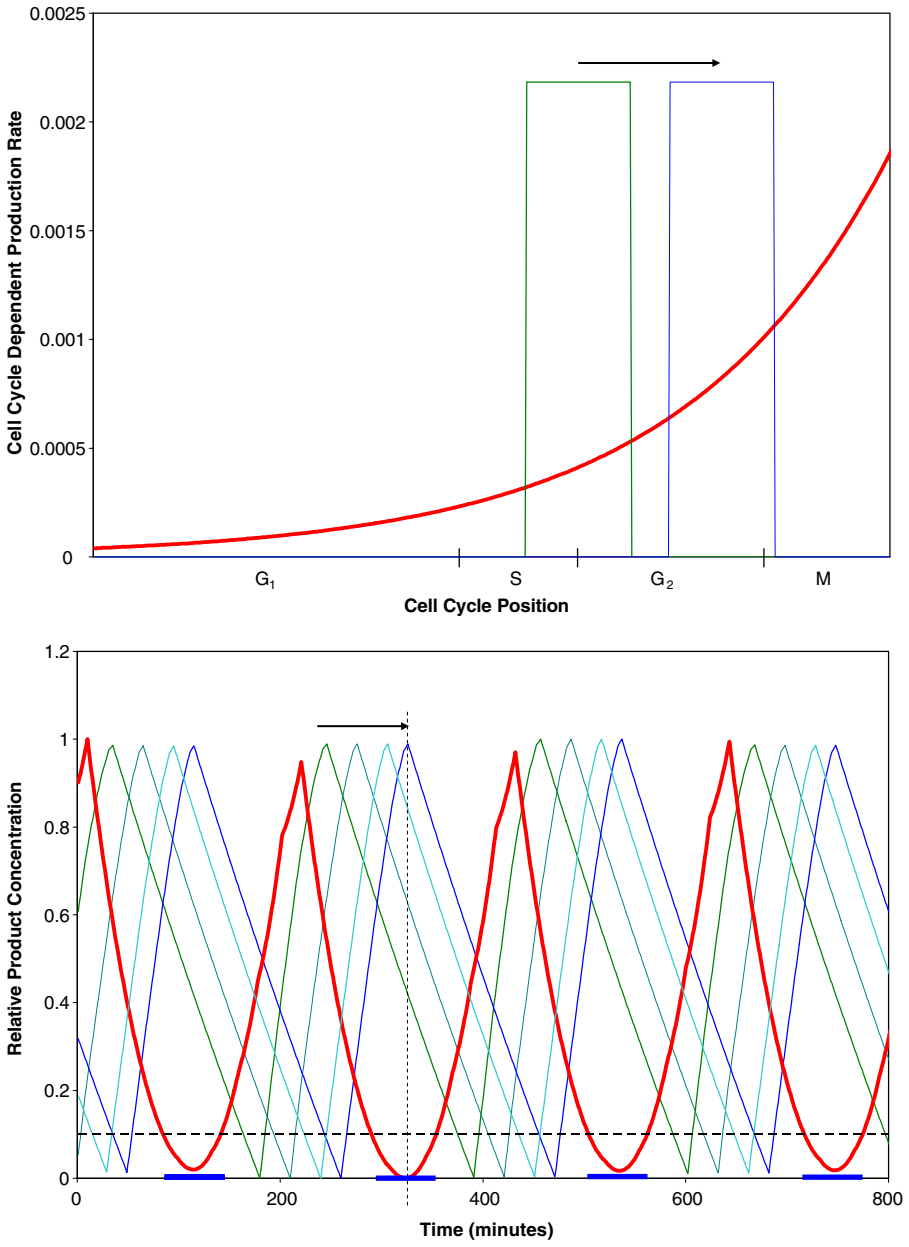

the upper panel and their matching accumulation signals in the bottom panel represent different choices for the desired product. As the simple square well expression profile is shifted along the cell cycle from green to blue, a maximum enrichment ratio occurs in the product relative to the ambient biocomplexity. This occurs when the accumulation profile of the ambient biocomplexity(red) is maximally out of phase with the accumulation profile of the product (blue to green).

The series of simulations shown in Fig. 8 amount to the equivalent of design equations. The theory shows that punctate expression profiles, such as the green and blue in the top panel of Fig. 8, tile the spectrum of possible phases. Therefore, if the ambient biocomplexity can be measured or accurately modeled, then a promoter design equation can be produced to circumvent it. The product or the product producing cells would then be harvested during appropriately chosen time windows within this periodic oscillation when the enrichment ratio is largest. Time windows corresponding to low complexity are shown in the bottom panel. Periodic harvesting is only the beginning of a far more comprehensive scheme.

Let T be the length of an oscillation. Assume that the harvesting windows have duration γ that is an integral divisor of the cell cycle period, $n\,\gamma = T$. Consider an entire period of the cell cycle tiled with n equal time windows of the duration of γ. This concept is illustrated in Fig. 9. Given n-reactors, each of which is sequentially out of phase by an amount gamma, the product accumulation can occur with maximal enrichment continuously. Imagine the autonomous periodic oscillation as a clock and the reactors as the numbers on a clock face. When the harvesting portion of the trajectory enters a given reactor, its effluent is collected into an ancillary reactor or collection vessel. As the harvesting trajectory leaves a reactor, it enters the next reactor in the sequence by design. Much has been made of the relationship of the autonomous oscillations to ultradian rhythms and clocks [26]. This continuous harvesting scheme brings that analogy to life as an engineering tool. We might consider the initialism: continuous long-term oscillating collection scheme: CLOCKS.

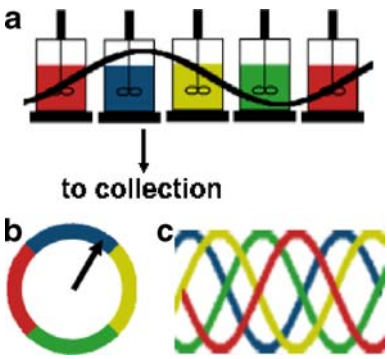

Fig. 9 The CLOCKS harvesting scheme. Suppose that the duration of an optimum harvesting window, γ, is one quarter of an oscillation. Then four systems prepared out phase tile a period. This is shown in **a**. Since a periodic oscillation can be thought of as a clock face, the sequence of color coded reactors correspond to the color coded clock face in **b**. The maximum enrichment ratio is depicted to occur at the peak of the oscillation shown to run through the system of reactors as a black curve. As the signal passes through the reactors, currently the blue reactor, the systems are bled in sequence as shown on the clock face. The sequence of windows, blue, yellow, green, red, blue…, is reiterated in **c** to indicate that in this scheme, product is continuously being harvested with a maximum enrichment ratio from the reactors in sequence

Conclusions

Downstream processing costs constitute the majority of the cost in product formation and accounts for over a tenfold increase in the price of biomanufactured goods [29]. Therefore, methods and methodologies of product enrichment are directly relevant to bioprocessing cost. We have argued that the ambient biocomplexity of a product within an admixture is the dominant contribution to processing cost. Our data and ideas imply that product enrichment can be achieved by co-opting the properties of autonomously oscillating yeast systems to minimize biocomplexity.

We have demonstrated that autonomously oscillating systems exhibit periodic oscillation in yield. We have shown that through an understanding of the population structure of periodically oscillating systems, we can increase product enrichment by interleaving product accumulation with the accumulation of its biocomplexity. Furthermore, we have described a novel phased, parallel, periodic harvesting method that is the direct engineering analogy of ultradian oscillations themselves: a continuous clock.

The ability to interleave product expression with that of its ambient biocomplexity rests on two pillars. The first is that the population structure of autonomous oscillations is marked by two observable and temporally coherent cell populations that traverse the cell cycle periodically. The second is the general flexibility afforded by the ability to genetically engineer cell-cycle-specific promoter expression. In mathematical abstraction, we have provided the proof of principle. What remains is a practical demonstration towards which the following issues exist. Promoters are not all of equal strength, and while phase is the dominant issue, the production of product above a necessary threshold may be challenging to engineer as a function of the cell cycle. If the cell is producing biomolecular mimics of the desired product at a rate several orders of magnitude larger at the maximum phase difference then, for that product, the interleaving strategy will have limited effect. The cell cycle and its implications for bioprocess control has already been recognized. Yeast have been engineered to produce amylase during the M-phase of the cell cycle [6]. It has been shown that heat shock arrest of the cells in M-phase, coupled with M-phase expression increased the yield of product. It remains to be seen if autonomously oscillating populations can outperform those in heat shock. Other work suggests that the efficiency of protein production is controlled by many factors other than promoter strength such as the protein sequence, fermentation temperature, and media composition [31].

Product enrichment from autonomous oscillations could also be used as a mechanism for simultaneous production of multiple products. If two or more products can be produced in different phases of the cell cycle, each product could be harvested during separate time windows and subjected to potentially different downstream processing. This could lead to savings on production equipment by eliminating the need for multiple fermentation setups.

Periodic sampling from autonomously oscillating systems was previously proposed as a means to increase yield above that provided by an equilibrium [14]. It could be argued that the value of such periodic sampling for product may be offset by the idle time of downstream processing equipment as opposed to continuous harvesting of a slightly smaller amount. This could be problematic for a continuous process that is not amenable to continual shutdown and start-up of equipment. However, the CLOCKS strategy that consists of a simple parallel array of oscillating systems whose phases are prepared to tile a period, as described in Fig. 9, completely and elegantly overcome these obstacles.

The physical chemistry of proteins is relatively well understood, and mature algorithms for their analysis exist along with large databases of known structures [32]. It is currently an active research interest in both basic science and in industry to develop theoretical tools to predict protein–protein interactions from an admixture [33]. With a solid understanding of cell-cycle-related protein expression, it should be possible over the course of the next decade to predict and manipulate the ambient biocomplexity of yeast.

Acknowledgments The authors would like to thank Peter Kotter from Johan Wolfgang Goethe-University for providing the yeast strain CEN.PK.113-7D and Rick Haselton for helpful discussion and generous use of his lab.

Appendix 1: Asymptotic Periodicity

Let the population density be periodic with period T. This means that $P(t+T,s) = p(t)$ for all s. From this, it follows that $I(t)$ is periodic with period T:

$$I(t+T) = \langle p(t+T,s), f(s)\rangle = \langle p(t,s), f(s)\rangle = I(t)$$

where we have used the inner product notation to represent the integrals from Eq. 4. Now consider the function $F(t)$. Using the well-known variation of parameters solution of Eq. 5, we have that

$$F(t) = e^{-Dt}\left[\int_0^t e^{Ds} I(s)\mathrm{d}s + C\right] \quad \text{where } C \text{ is an integration constant.}$$

Using the periodicity of I, we have:

$$\begin{aligned} F(t+T) &= e^{-Dt}\left[\int_0^{t+T} e^{D(s-T)} I(s)\mathrm{d}s + C\right] \\ &= e^{-Dt}\left[\int_0^{t+T} e^{D(s-T)} I(s-T)\mathrm{d}s + C\right] \\ &= e^{-Dt}\left[\int_{-T}^{t} e^{Ds} I(s)\mathrm{d}s + C\right] \\ &= e^{-Dt}\left[\int_{-T}^{t} e^{Ds} I(s)\mathrm{d}s + \int_{-T}^{0} e^{Ds} I(s)\mathrm{d}s + C\right] \\ &= F(t) + e^{-Dt}\int_{-T}^{t} e^{Ds} I(s)\mathrm{d}s \end{aligned}$$

Since the last integrand is finite and e^{-Dt} limits to 0 exponentially as t goes to ∞, $F(t)$ is an asymptotically periodic with period T.

Appendix 2: Leslie Model of Yeast Growth and Division

$$\begin{bmatrix} f_0^0(t+\tau_0) \\ f_1^0(t+\tau_1) \\ f_2^0(t+\tau_2) \\ \vdots \\ f_n^0(t+\tau_n) \end{bmatrix} = \begin{bmatrix} 1 & 1 & 1 & \cdots & 1 & 1 \\ 1 & 0 & 0 & \cdots & 0 & 0 \\ 0 & 1 & 0 & \cdots & 0 & 0 \\ \vdots & \vdots & \vdots & \ddots & \vdots & \vdots \\ 0 & 0 & 0 & \cdots & 1 & 0 \end{bmatrix} \begin{bmatrix} f_0^0(t) \\ f_1^0(t) \\ f_2^0(t) \\ \vdots \\ f_n^0(t) \end{bmatrix}$$

where:

$$\left\{ \begin{array}{l} f_{\text{in}}^i(t) = \text{Total flux entering the } i-th \text{ generation at time } t \\ f_i^0(t) = \text{Daughter cells produced from a division in age class } i \text{ at time } t \\ \tau_i = \text{Flux residence time, i.e. cell cycle length} \end{array} \right\}.$$

The Leslie model [16] used to calculate yeast growth and division encodes as a mathematical object the process flow depicted at the top of Fig. 10. The process flow has age descending from daughter cells with no scars, P_0, at the top to cells with arbitrarily many scars, P_n, at the bottom. Cells belonging to each of these age classes traverse their separate cell cycles, shown as the horizontal thick black lines. The time it takes a cell of age, k, to traverse their cell cycle is τ_k. The values of τ used are shown in Table 3 along

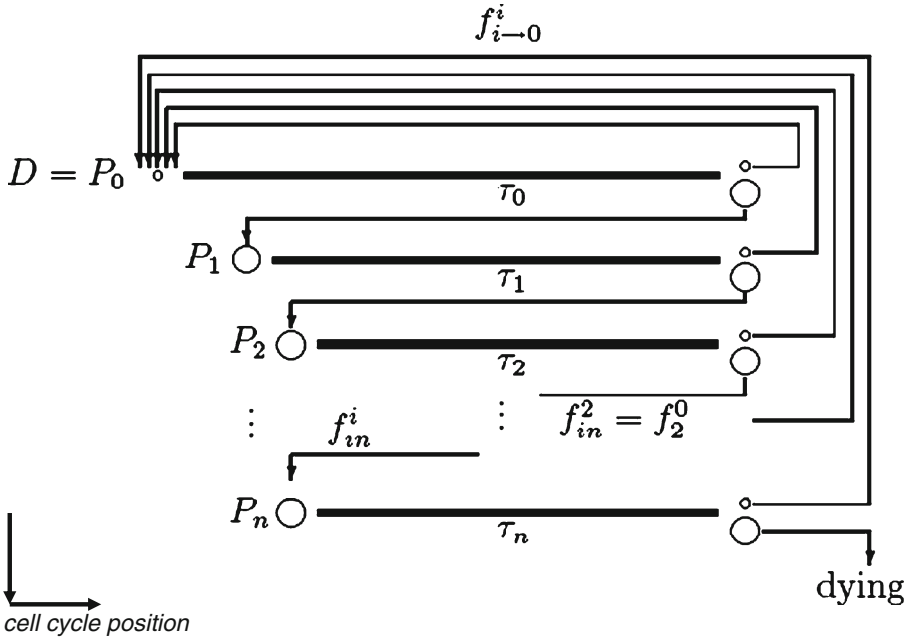

Fig. 10 The top schematic represents the process of yeast growth and division. Each age class is represented by a *bold horizontal line* and corresponding residence time, τ. The age classes are organized by replicative age, with the daughter cells, denoted P_0, as the first grid. Higher generation parent cells are listed below. Each cell division can be characterized by producing a daughter cell back at the beginning of the P_0 grid and a parent of the next highest age class. This process can be represented by a Leslie matrix as shown by the *bottom panel*

Table 3 Parameters used in the Leslie model simulations.

Leslie model parameters				
Age class	T	BE	S-phase end	G_2-phase end
P_0	522	261	362	457
P_1	483	241	302	423
P_2	437	219	273	383
P_3	398	199	249	349
P_4	347	174	217	304
$P_{5–9}$	277	138	173	242

The parameters are listed in order of replicative age. Cell cycle duration and progression can be described in terms of time. Parameters are described in units of minutes

with the temporal position of bud emergence. The thin black lines with arrows indicate the directions of possible flux due to cell divisions. Each arrow corresponds to a 1 in the matrix representation of the process at the bottom of Fig. 10.

Given an initial population distribution, the matrix model is iterated to produce the dynamics. Typically, such a system would produce asynchronous exponential growth. Autonomous oscillations result from an additional feedback. We have introduced a *delay model* to produce population oscillation. In the delay model, a threshold, T_R, is introduced. Once the density of cell in the S-phase of the cell cycle reaches T_R or above, any cells in a 10% strip proximal to S become delayed in their cell cycle progression. In the simulations described in Fig. 8, T_R was 20% of the total culture density. The S-phase is delimited on the left by bud emergence (BE) as described in Table 3. The algorithm used to implement this model is freely available from the authors upon request.

References

1. Dumas, B., Masson, C., Lebrun, K., & Achstetter, T. (2006). Hydrocortisone made in yeast: metabolic engineering turns a unicellular microorganism into a drug-synthesis factory. *Biotechnology Journal*, *1*, 299–307.
2. Kjeldsen, T., Ludvigsen, S., Diers, I., Balshmidt, P., Sorensen, A., & Kaarshold, N. (2002). Engineering-enhanced protein secretory expression in yeast with applications to insulin. *Journal of Biological Chemistry*, *277*, 18245–18248.
3. Szczebara, F., Changelier, C., Villeret, C., Masurel, C., Masurel, A., Bourot, S., et al. (2003). Total biosynthesis of hydrocortisone from a simple carbon source in yeast. *Nature*, *21*, 143–149.
4. Thim, L., Hansen, M., Norris, K., Holegh, I., Boel, E., Forstrom, J., et al. (1986). Secretion and processing of insulin precursors in yeast. *PNAS*, *83*, 6766–6770.
5. Chan, E., Chen, C., & Chen, L. (1992). Recovery of invertase from ethanol fermentation broth. *Biotechnology Letters*, *14*, 573–576.
6. Uchiyama, K., Morimoto, M., Yokoyama, Y., & Shioya, S. (1996). Cell cycle dependency of rice α-amylase production in a recombinant yeast. *Biotechnology and Bioengineering*, *54*, 262–271.
7. Bansal, V., Roychoudhurry, P., Mattiasson, B., & Kumar, A. (2006). Recovery of urokinase from integrated mammalian cell culture cryogel bioreactor and purification of the enzyme using *p*-aminobenzamidine affinity chromatography. *Journal of Molecular Recognition*, *19*, 332–339.
8. Sajc, L., Grubisic, D., & Novakovic, G. (2000). Bioreactors for plant engineering: An outlook for further research. *Biochemical Engineering Journal*, *4*, 89–99.
9. Smith, C. (2005). Striving for purity: Advances in protein purification. *Nature*, *2*, 71–77.
10. Stowers, C., & Boczko, E. M. (2007). Reliable cell disruption in yeast. *Yeast*, *24*, 533–541.
11. Gleeson, M., White, C., Meininger, D., & Komives, A. (1998). Generation of protease-deficient strains and their use in heterologous protein expression. *Methods in Molecular Biology*, *103*, 81–94.

12. Alberghina, L., Mariani, L., Martegani, E., & Vanoni, M. (1983). Analysis of protein distribution in budding yeast. *Biotechnology and Bioengineering*, *15*, 1295–1310.
13. Vanoni, M., Vai, M., Popolo, L., & Alberghina, L. (1983). Structural heterogeneity in populations of budding yeast *Saccharomyces cerevisiae*. *Journal of Bacteriology*, *156*, 1282–1291.
14. Hortso, M. (1996). Population balance models of autonomous periodic dynamics in microbial cultures: Their use in process optimization. *Canadian Journal of Chemical Engineering*, *74*, 612–620.
15. Walker, G. (1999). Synchronization of yeast cell populations. *Methods in Cell Science*, *21*, 87–93.
16. Stowers, C., Hackworth, D., Mischaikow, K., Gedeon, T., & Boczko, E. (2008). Extending synchrony and deconvolving population effects in budding yeast through an analysis of volume growth with a structured Leslie model. *Theoretical Population Biology* (in press).
17. Richard, P. (2003). The rhythm of yeast. *FEMS Microbiology Reviews*, *27*, 547–557.
18. Dawson, P. (1972). Continuous synchronous culture—The production of extracellular enzymes by continuous phased culture of *Bacillus subtilis*. *Proceedings of the IV IFS: Ferment. Technol. Today*, pp. 121–128.
19. Jules, M., Francois, J., & Parrou, J. (2005). Autonomous oscillations in *Saccharomyces cerevisiae* during batch cultures of trehalose. *FEBS Journal*, *272*, 1490–1500.
20. Bellgardt, K. H. (1994). Analysis of synchronous growth of bakers yeast. Part I: Development of a theoretical model for sustained oscillations. *Journal of Biotechnology*, *35*, 19–33.
21. Bellgardt, K. H. (1994). Analysis of synchronous growth of bakers yeast. Part II: Development of a theoretical model for sustained oscillations. *Journal of Biotechnology*, *35*, 35–49.
22. Beuse, M., Bartling, R., Kopmann, A., Deikmann, H., & Thoma, M. (1998). Effect of the dilution rate on the mode of oscillation in continuous cultures of *Saccharomyces cerevisiae*. *Journal of Biotechnology*, *61*, 15–31.
23. Crooke, P., Tanner, R., & Park, D. (1986). Time dependent differential yield as a scale-up parameter in enzyme and fermentation reactors. *Biotechnology Progress*, *2*, 40–47.
24. Essajee, C., & Tanner, R. D. (1979). The effect of extracellular variables on the stability of continuous baker's yeast–ethanol fermentation process. *Process Biochemistry*, *25*, 16–21.
25. Heinzle, E., Dunn, I., Furukawa, K., & Tanner, R. D. (1982). Modeling of sustained oscillations observed in continuous culture of *Saccharomyces cerevisiae*. In A. Halme (Ed.), *Proceedings of the 1st IFAC Workshop* (pp. 57–65). Oxford: Pergamon.
26. Murray, D., Klevecz, R., & Lloyd, D. (2003). Generation and maintenance of synchrony in *Saccharomyces cerevisiae* continuous culture. *Experimental Cell Research*, *287*, 10–15.
27. Tu, B. P., Kudlicki, A., Rowicka, M., & McKnight, S. L. (2006). Logic of the yeast metabolic cycle: Temporal compartmentalization of cellular processes. *Science*, *310*, 1152–1158.
28. Xu, Z., & Tsurugi, K. (2006). A potential mechanism of energy-metabolism oscillation in an aerobic chemostat culture of the yeast *Saccharomyces cerevisiae*. *FEBS Journal*, *273*, 1696–1709.
29. Aldridge, S. (1996). Downstream processing needs a boost. *Genetic Engineering and Biotechnology News*, *26*, 1.
30. Ramesh, M., Charyulu, N., Chand, N., & Lonsane, B. (2004). Non-growth associated production of enzymes in solid state fermentation systems: Its mathematical description for two enzymes produced by *Bacillus licheniformis*. *Bioprocess and Biosystems Engineering*, *15*, 289–294.
31. Cos, O., Ramon, R., Luis Montesinos, J. L., & Valero, F. (2006). Operational strategies, monitoring and control of heterologous protein production in the methylotrophis yeast *Pichia pastoris* under different promoters: a review. *Microbial Cell Factories*, *5*, 17.
32. Taufer, M., An, C., Kerstens, A., & Brooks, C. (2006). Predictor @ home: A "protein structure prediction supercomputer" based on global computing. *IEEE Transactions on Parallel and Distributed Systems*, *17*, 786–796.
33. Qui, J., & Noble, W. (2008). Predicting co-complexed protein pairs from heterogeneous data. *PLOS Computation Biology*, *4*, e1000054.
34. Hartwell, L. (1974). *Saccharomyces cerevisiae* cell cycle. *Bacteriological Reviews*, *38*, 164–198.
35. Hartwell, L., & Unger, M. (1977). Unequal division in *Saccharomyces cerevisiae* and its implications for the control of the cell division. *Journal of Cell Biology*, *75*, 422–435.